Southern Argentina Agile Meteor Radar: System design and initial measurements of large-scale winds and tides

D. C. Fritts,[1] D. Janches,[1] H. Iimura,[1] W. K. Hocking,[2] N. J. Mitchell,[3] R. G. Stockwell,[1] B. Fuller,[4] B. Vandepeer,[4] J. Hormaechea,[5] C. Brunini,[6] and H. Levato[7]

Received 11 January 2010; revised 16 April 2010; accepted 28 April 2010; published 22 September 2010.

[1] The Southern Argentina Agile Meteor Radar (SAAMER) was installed at Rio Grande on Tierra del Fuego (53.8°S, 67.8°W) in May 2008 and has been operational for ~24 months. This paper describes the motivations for the radar design and its placement at the southern tip of South America, its operating modes and capabilities, and observations of the mean winds, planetary waves, and tides during its first ~20 months of operation. SAAMER was specifically designed to provide very high resolution of large-scale motions and hopefully enable direct measurements of the vertical momentum flux by gravity waves, which have only been possible previously with dual- or multiple-beam radars and lidars or in situ measurements. SAAMER was placed on Tierra del Fuego because it was a region devoid of similar measurements, the latitude was anticipated to provide high sensitivity to an expected large semidiurnal tide, and the region is now recognized to be a "hot spot" of small-scale gravity wave activity extending from the troposphere into the mesosphere and lower thermosphere, perhaps the most dynamically active location on Earth. SAAMER was also intended to permit simultaneous enhanced meteor studies, including "head echo" and "nonspecular" measurements, which were previously possible only with high-power large-aperture radars. Initial measurements have defined the mean circulation and structure, exhibited planetary waves at various periods, and revealed large semidiurnal tide amplitudes and variability, with maximum amplitudes at higher altitudes often exceeding 60 m s^{-1} and amplitude modulations at periods from a few to ~30 days.

Citation: Fritts, D. C., et al. (2010), Southern Argentina Agile Meteor Radar: System design and initial measurements of large-scale winds and tides, *J. Geophys. Res.*, *115*, D18112, doi:10.1029/2010JD013850.

1. Introduction

[2] The structure and variability of the mesosphere and lower thermosphere (MLT) is determined to a large degree by large- and small-scale waves propagating into this region from below. Both large-scale motions, comprising various tidal components and planetary waves (PWs) having periods of ~2 to 30 days, and smaller-scale gravity waves (GWs), exhibit significant variability with season and latitude because of the seasonal variations in their sources and propagation environments [e.g., *Holton*, 1984; *Burrage et al.*, 1995; *Vincent et al.*, 1998; *Manson et al.*, 1999: *Pancheva et al.*, 1999; *McLandress*, 2002; *Fritts and Alexander*, 2003]. GWs and tides also exhibit longitudinal variability reflecting the longitudinal distributions of their forcing dynamics [e.g., *Tsuda et al.*, 2000; *Hagan and Forbes*, 2002, 2003; *Espy et al.*, 2006]. Indeed, there are preferred latitudes and longitudes where these various motions systematically achieve their largest responses.

[3] Possibly the most dramatic response occurs during austral winter and extends from southern South America over the Drake Passage and the Antarctic Peninsula, spanning latitudes from 30°W to 70°S and longitudes from ~30°S to 80°W. The migrating semidiurnal tide achieves maximum amplitudes in the MLT from ~40°S to 70°S during winter [*Hagan and Forbes*, 2003], while GW variances and momentum flux estimates typically exhibit strong maxima at these locations extending from the lower stratosphere into the MLT [*McLandress et al.*, 2000; *Ern et al.*, 2004; *Wu*, 2004; *Jiang et al.*, 2006; *Alexander et al.*, 2008a; *Wu and Eckermann*, 2008]. In several cases, the sources of these motions are clearly linked to the high terrain of the Andes and the Antarctic Peninsula [*Jiang et al.*, 2002; *Preusse et al.*, 2002,

[1]NorthWest Research Associates, Colorado Research Associates division, Boulder, Colorado, USA.
[2]Department of Physics, University of Western Ontario, London, Ontario, Canada.
[3]Center for Space, Atmosphere and Oceanic Science, Department of Electronic and Electrical Engineering, University of Bath, Bath, Avon, UK.
[4]Genesis Software Pty Ltd., Adelaide, South Australia, Australia.
[5]Estacion Astronomica Rio Grande (EARG), Universidad Nacional de La Plata (UNLP), Consejo Nacional de Investigaciones de Ciencoa y Tecnica (CONICET), San Juan, Argentina.
[6]Facultad de Ciencias Astronómicas y Geofísicas, UNLP/CONICET, San Juan, Argentina.
[7]Instituto de Ciencias Astronomicas, de la Tierra y del Espacio (ICATE)/CONICET, San Juan, Argentina.

Copyright 2010 by the American Geophysical Union.
0148-0227/10/2010JD013850

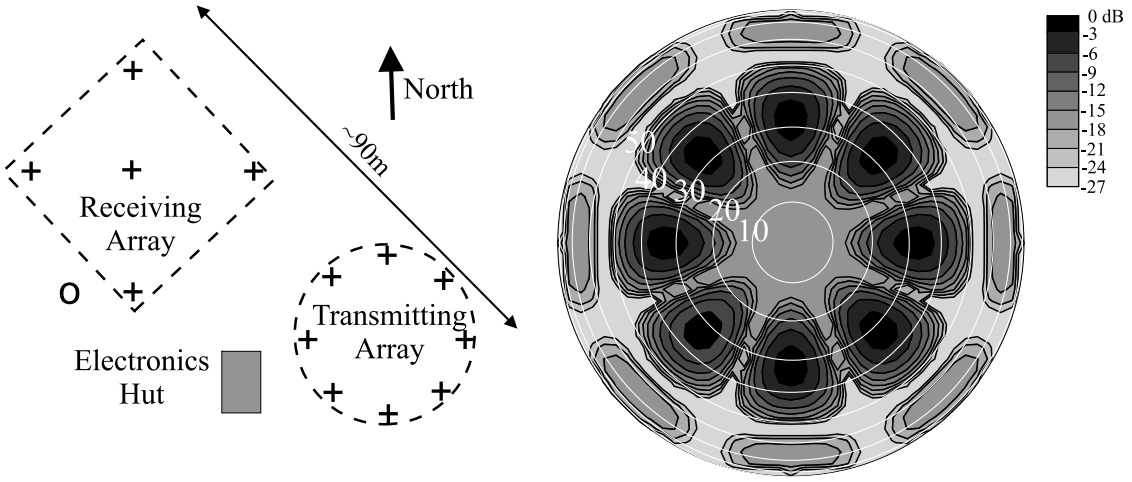

Figure 1. (left) Antenna transmitter and receiver layout at Rio Grande, Tierra del Fuego (with individual antennas indicated with plus symbols) and (right) the anticipated beam pattern polar diagram. The resulting beams have peak sensitivity at ~35° off zenith.

2006; *Wu and Jiang*, 2002; *Eckermann et al.*, 2006; *Wu et al.*, 2006; *Alexander et al.*, 2008b; *Hertzog et al.*, 2008]. Limited data also indicate penetration of mountain waves (MWs) to altitudes approaching ~100 km under suitable propagation conditions [*Smith et al.*, 2009]. But these sources do not obviously account for the large variances and inferred fluxes over the Drake Passage, suggesting that jet stream shears and flow imbalances may also contribute significantly to enhanced GWs in this region [e.g., *Guest et al.*, 2000].

[4] These dynamics and our expectation for strong interactions among the various motions were the motivation for placing the Southern Argentina Agile Meteor Radar (SAAMER) at Rio Grande on Tierra del Fuego (53.8°S, 67.8°W) in May 2008. SAAMER was specifically designed to provide the potential to directly measure the anticipated GW-tidal and GW-PW interactions and their modulation of GW variances and momentum fluxes, which have been observed in limited MLT observations [*Fritts and Vincent*, 1987; *Wang and Fritts*, 1991; *Thayaparan et al.*, 1995; *Isler and Fritts*, 1996; *Manson et al.*, 1998; *Murphy and Vincent*, 1998; *Espy et al.*, 2004] and in numerical models of these dynamics [*Holton*, 1984; *Miyahara*, 1985; *Miyahara et al.*, 1986; *Forbes et al.*, 1991; *Lu and Fritts*, 1993; *Meyer*, 1999], but which have yet to be fully quantified, understood, and adequately parameterized in large-scale models [*McLandress and Ward*, 1994; *McLandress*, 1998, 2002; *Hagan et al.*, 1999; *Fritts and Alexander*, 2003].

[5] Our purposes in this paper are to describe the SAAMER radar system and measurement capabilities and its measurements of large-scale dynamics at MLT altitudes throughout its first ~20 months of operation. The radar configuration, the spatial and temporal variations of meteor detections observed from Rio Grande, and our data analysis methods are described in section 2. Mean and PW wind fields throughout the first ~16 months of observations are described in section 3. Section 4 describes the monthly and daily variability of the diurnal and semidiurnal tidal amplitudes on seasonal and PW times scales. Section 5 provides a comparison of our measured tidal amplitude and phase structures with the Global-Scale Wave Model, version 2002 (GSWM-02) [see *Hagan and Forbes*, 2002, 2003], and a discussion of other similar comparisons by other authors using various radar and satellite data sets. A summary and conclusions are provided in section 6. Companion papers by *Fritts et al.* [2010] and Beldon et al. (C. L. Beldon, et al., Gravity wave variances and tidal interactions inferred with SAAMER (53.8°S, 67.8°W), manuscript in preparation, 2010) describe assessments of GW momentum fluxes and GW variances and their modulation by tidal motions that are also enabled by the SAAMER radar.

2. SAAMER System Description and Data Collection and Analysis

[6] The SAAMER radar was specifically designed to enable very high resolution definition of the large-scale wind field and potential sensitivity to GW momentum fluxes employing a generalization of the dual-beam technique first employed by *Vincent and Reid* [1983] and subsequently for multiple-beam studies by *VanZandt et al.* [1990] and *Fritts et al.* [1990]. To define both the large-scale motion field at high resolution and enable estimates of GW momentum fluxes, it is necessary to achieve high meteor count rates at sufficiently small off-zenith angles to allow vertical motions due to GWs to make significant contributions to the inferred radial velocities. This was accomplished through significantly higher peak power than employed by typical meteor radars (60 kW rather than ~5–15 kW) and using a novel transmitting array that directs the majority of radar power into eight beams at 45° azimuth increments with peak power at ~35° off zenith and a majority of meteor detections at off-zenith angles between 15° and 50°. The SAAMER antenna design and anticipated spatial sensitivity are shown schematically in Figure 1. The distribution of unambiguous meteor detections achieving a threshold accuracy (>12,000 meteors and ~50% of the total detections) for 20 May 2008 is

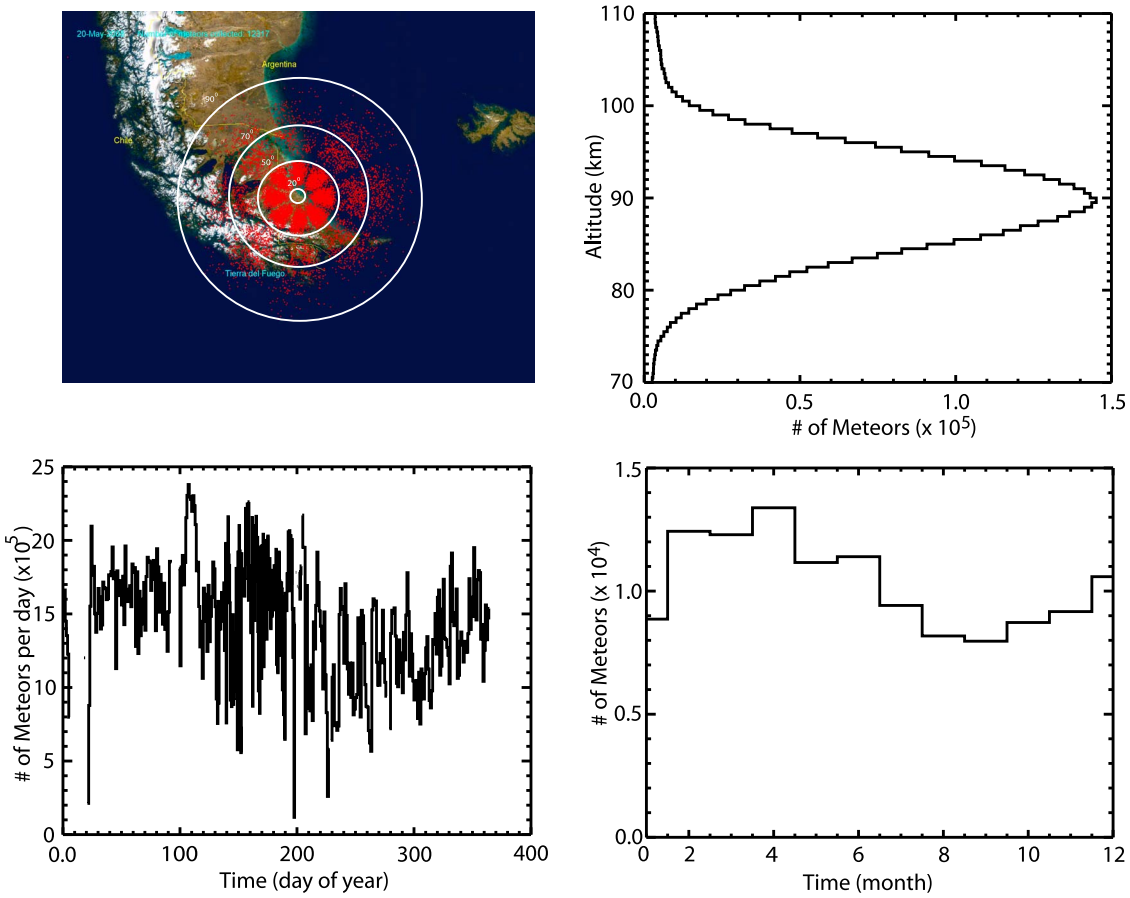

Figure 2. (top left) SAAMER meteor detections above our acceptable detection threshold (total = 12,317) for 20 May 2008, (top right) mean meteor distribution with altitude, and (bottom left and right) daily and monthly counts throughout the annual cycle. White circles at top left show locations at 50°, 70°, and 90° off zenith. The majority of meteors are detected at zenith angles <50° and the primary beam lobes are centered at ~35° off zenith and aligned with and midway between the cardinal directions.

shown in Figure 2. Primary radar parameters and measurement capabilities include the following:

[7] 1. a radar frequency and bandwidth of 32.55 and 0.3 MHz, respectively;

[8] 2. a transmitter antenna composed of eight three-element crossed yagis in a circle of diameter 27.6 m having opposite phasing of every other yagi (normal mode);

[9] 3. five receiver channels to enable redundant meteor position definition;

[10] 4. a transmit/receive (T/R) switch allowing both tropospheric measurements and use of the transmitter antenna as a sixth receiver;

[11] 5. a transmitter phasing option that allows power to be directed vertically, enabling neutral vertical velocity measurements in the troposphere and MLT; and

[12] 6. sufficient power and beam definition flexibility to perform enhanced meteoroid radiant, population size, and "head echo" studies normally possible only with high-power, large-aperture (HPLA) radars.

[13] For our initial studies, SAAMER employed a single 13 μs pulse (yielding a 2 km range bin), a pulse repetition frequency of 2144 Hz, an integration over four samples, and meteors detections at altitudes from 70 to 110 km. SAAMER also has options for pulse coding that we have recently implemented and which will increase meteor counts in future measurements.

[14] Mean and large-scale winds are determined by fitting a mean horizontal wind in each 3 km altitude bin to each hour of meteor radial velocities at off-zenith angles between 15° and 50°. Spectra of the zonal and meridional winds obtained from these data are shown for the first year of SAAMER measurements in Figure 3. These reveal broad maxima near the inertial period in both spectra (~14.9 h), as well as significant responses at the 24, 12, 8, and 6 h tidal periods and PW periods of ~16–30 days in the zonal component and at the 24, 12, and 8 h tidal periods and PW periods of ~2–16 days in the meridional component. Spectra provide no information on the seasonal behavior or temporal extent of these various motions, however.

[15] To examine this behavior further, hourly winds are also employed to infer local diurnal, semidiurnal, and residual mean zonal and meridional winds employing an "S transform" Gaussian wavelet fit to the diurnal and semidiurnal periods having wavelet widths equal to the respective tidal periods [*Stockwell et al.*, 1996]. This yields daily estimates of the diurnal and semidiurnal tidal amplitudes and a residual

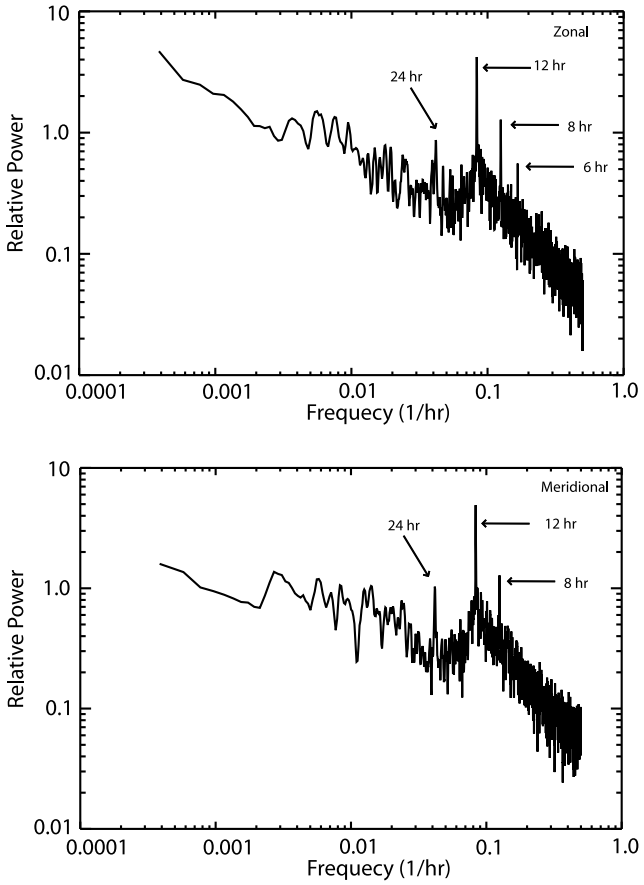

Figure 3. (top) Zonal and (bottom) meridional spectra of hourly winds obtained with SAAMER at 88.5 km for the first year of measurements extending from May 2008 to May 2009. A 5-point triangular smoothing is applied to delineate the tidal and PW peaks more clearly.

mean motion field that exhibits variability on seasonal and shorter PW time scales. A test of this method was performed for a wind field composed of (1) constant mean zonal and meridional motions, (2) a constant diurnal tide amplitude (20 m s^{-1}) with altitude and time, and (3) a semidiurnal tide having both a constant amplitude (20 m s^{-1}) and a time- and altitude-varying amplitude (with the total varying linearly from 20 to 60 m s^{-1} from 80 to 100 km and modulated by a 10 day period) mapped to the actual meteor distributions in space and time for September 2008. The zonal tidal retrievals are shown together with the specified winds at altitudes from 76.5 to 97.5 km in Figure 4 and reveal amplitude estimates within 10% or less except at the lowest and highest altitudes displayed, even for the highly variable semidiurnal amplitudes. Results of this analysis are described in the following two sections. Similar evaluations of the retrieval of GW momentum fluxes for various propagating and stationary GWs in the presence of various mean and tidal wind fields for both test and observed meteor distributions are described by *Fritts et al.* [2010] and suggest confidence in the SAAMER ability to define these fields for monthly assessments of mean and tidal modulation of these fluxes. Finally, to compare our tidal assessments with the GSWM-02 model, we also fit monthly data with a single tidal amplitude and phase for consistency with other authors.

3. Mean and Planetary Wave Wind Fields

[16] Time-height cross sections of monthly and daily mean zonal and meridional winds are displayed in the top and middle frames of Figure 5. Monthly mean zonal winds (top left) are eastward for most altitudes between 80 and 98 km for most of the annual cycle. Maximum values are ~30 m s^{-1} in July 2008 ~85–95 km, in February 2009 at ~90 km, and in August 2009 above ~90 km. Westward monthly mean winds occur only from October 2008 into February 2009 at 80 km, exhibit a westward maximum of ~40–45 m s^{-1} in November and December 2008 at this altitude, are more restricted in time at higher altitudes, and exhibit a reversal at ~91 km. Monthly mean eastward winds are small, ~10 m s^{-1} or less, above the summer westward jet extending to ~95 km in October 2008, at altitudes of ~95 km and above in June 2009, above ~90 km in March and April 2009 (and penetrating as low as ~83 km in April), and above ~90 km in July 2009. For most of the year and most altitudes, monthly mean zonal winds appear more strongly eastward than at similar Northern Hemisphere latitudes [*Avery et al.*, 1989; *Portnyagin et al.*, 2004, 2006; *Dowdy et al.*, 2007]. We note below, however, that zonal winds (and monthly means) are strongly modulated by various PWs having deep, coherent responses of ~10–15 km in altitude, especially from about May to September.

[17] In contrast to the mean zonal winds, monthly mean meridional winds (Figure 5, top right) are relatively weak, ~15 m s^{-1} or less for much of the year. Small variability is seen extending from November 2008 into March 2009, with northward maxima of ~15 m s^{-1} at ~92 km in December 2008 and ~10 m s^{-1} from ~81 to 86 km in February 2009. Larger winds and variability accompany southward mean winds (at some altitudes) extending from May into October 2008 and from March 2009 to the end of our data set in September 2009. Southward mean winds occur in May, July, and September of 2008 at all altitudes observed, with additional weak southward mean winds during March and April of 2009 and stronger southward maxima of ~20–35 m s^{-1} at higher altitudes during May and August of 2009. As noted above for the zonal mean winds, however, monthly mean meridional winds are seen below to be largely dictated by PW motions having larger and variable amplitudes.

[18] Daily mean zonal and meridional winds (Figure 5, middle) exhibit considerable variability not captured in the monthly mean wind fields that are indicative of various PW structures. These features have maximum winds about twice as large as seen in the monthly mean winds (frequently 40–50 m s^{-1}, with maxima approaching 70 m s^{-1}), which typically exhibit coherence over altitudes of ~10–15 km.

[19] To examine the variability of zonal and meridional mean winds on PW time scales, we show S transforms of hourly estimates of the daily mean zonal and meridional wind fields in the third frames of Figure 5. The most significant maxima occur at periods of ~1.8 and ~3 days from late January into February and from late February into March 2009, respectively, with comparable amplitudes in the two fields during the first interval but a larger response in the meridional wind field during the second. Smaller maxima are

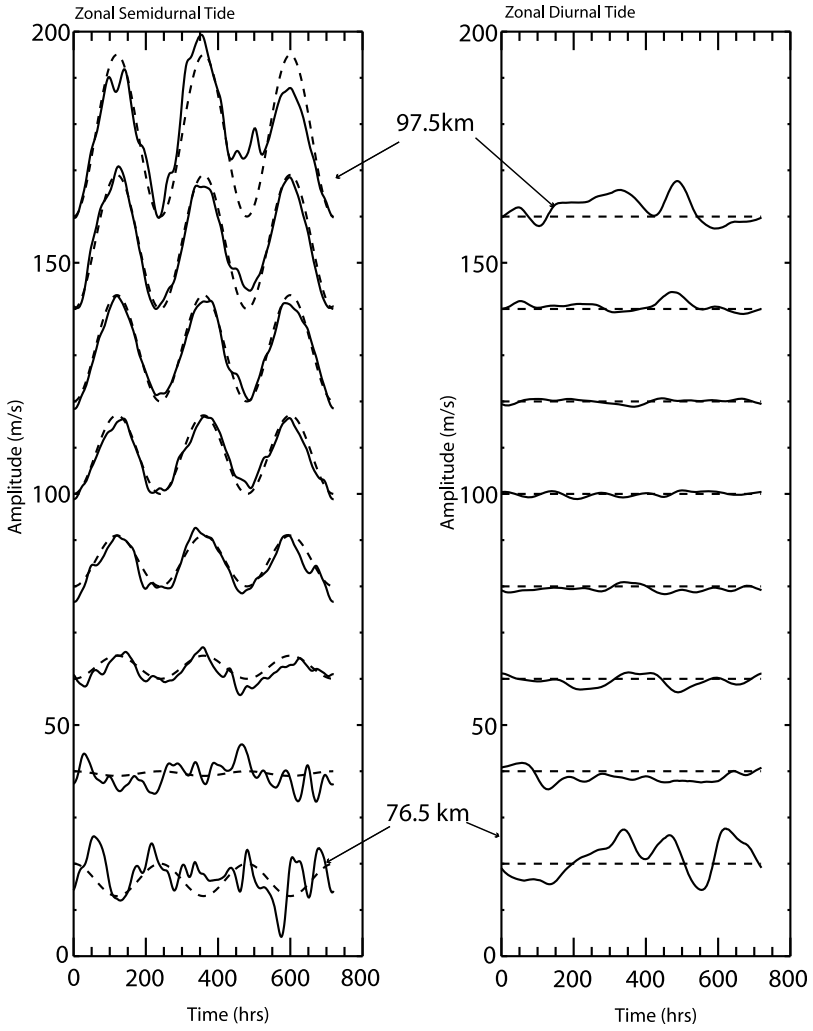

Figure 4. Test zonal (left) semidiurnal and (right) diurnal tidal retrievals employing the S transform for specified winds at observed meteor locations and times during September 2008. Specified and retrieved amplitudes are shown with dashed and solid lines in each case. Note that retrieved values have errors of ~10% or less from ~80 to 95 km for daily estimates where meteor counts in an altitude bin are ~40% of the maximum value. Errors are much smaller in defining month mean amplitudes and phases.

also seen throughout the year, with the primary responses in the zonal wind during these events. These appear to be signatures of the quasi 2 day wave, which occurs in both northern and southern hemispheres and can depart significantly from a 2 day period depending on the zonal wave number accounting for the response [*Pancheva et al.*, 2004, 2006; *Murphy et al.*, 2007; *Baumgaertner et al.*, 2008].

[20] PW wind variations at longer periods, ~4–30 days, typically exhibit several superposed periods, event durations of several cycles, and apparent correlations between events having different periods. The meridional S transform suggests that ~16 day periods often precede ~3 day events (see the interval from about June through October 2008), while the zonal S transform suggests that ~3 day motions often accompany or precede ~5–6 day motions, ~5–6 day motions often accompany ~8–16 day motions, and ~16 day motions more nearly alternate with lower-frequency motions. There are also suggestions that some PW events undergo an evolution to shorter or longer periods in a nearly continuous manner. Finally, 2 day averaged winds for 2009 band-passed from 5 to 20 and from 15 to 60 days (Figure 5, bottom) reveal that the relationships between PW zonal and meridional winds range from quadrature (with either component leading) to in phase and antiphase, suggesting significant variability in PW structure and strong PW mean flow interactions. Indeed, the PW structures revealed in this cursory analysis are highly variable and interesting in their own right. This analysis is beyond the scope of this paper and will be presented a separate paper that evaluates these structures employing data from SAAMER and a conjugate northern latitude site.

4. Tidal Motions

4.1. Diurnal Tide

[21] Time-height cross sections of monthly mean and daily diurnal tide zonal and meridional wind amplitudes are displayed in the top four frames of Figure 6. Monthly mean amplitudes (top) exhibit significant seasonal and altitude variability, suggesting a superposition of migrating and nonmigrating modes having different vertical structures that

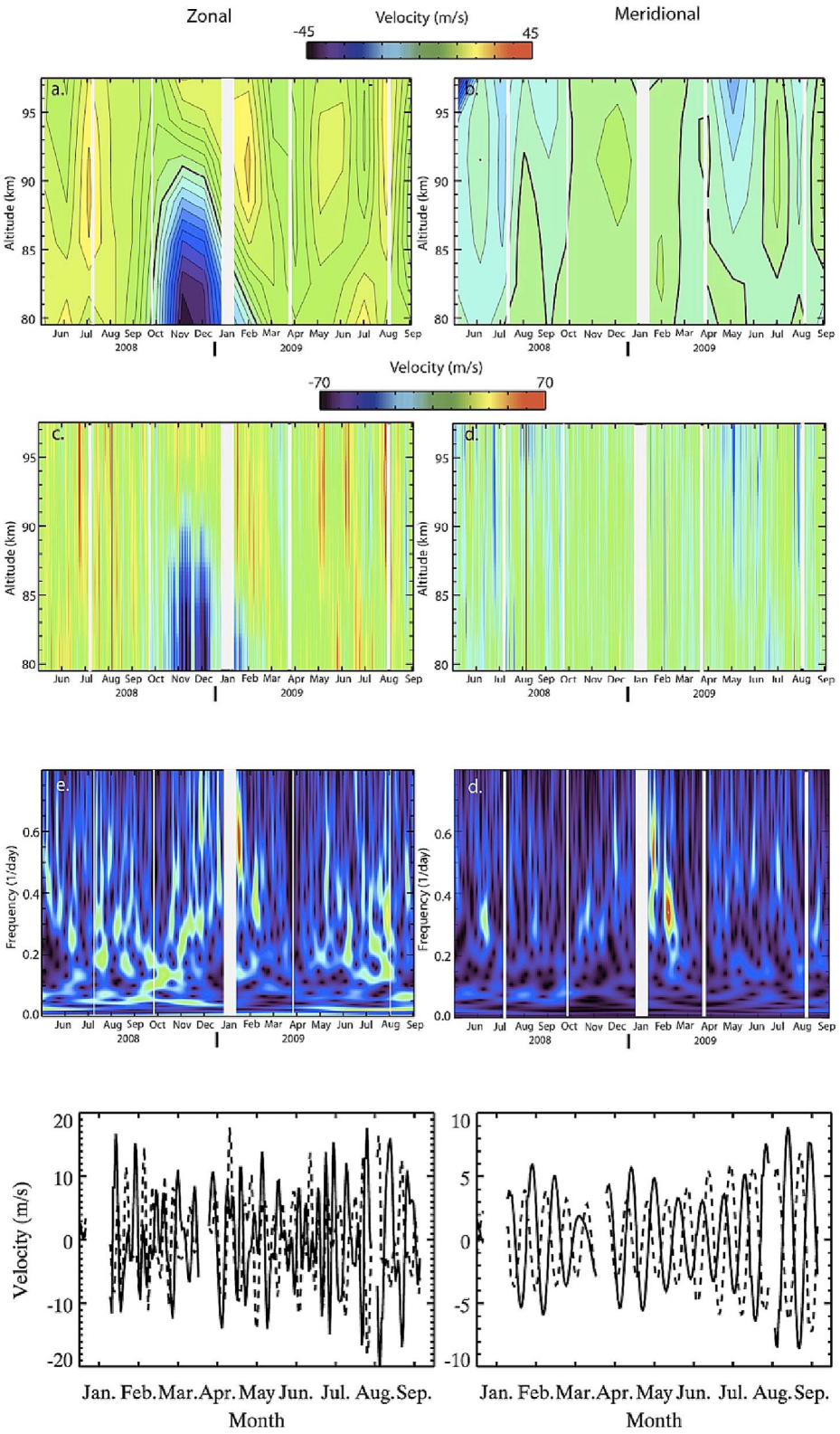

Figure 5. (top frames) Monthly mean and (second frames) daily mean (left) zonal and (right) meridional winds from May 2008 to September 2009. The third frames display S transforms of the zonal and meridional daily mean winds at 88.5 km (left and right). Note the significant ~2 day response in January and February 2009 and the tendency for the dominant PW responses at longer periods in the zonal wind. The bottom frames display zonal (solid) and meridional (dashed) 2 day averaged 2009 winds band-passed at 5–20 and 15–60 days (left and right). Data gaps longer than 1 day are shown as blank intervals in the colored frames.

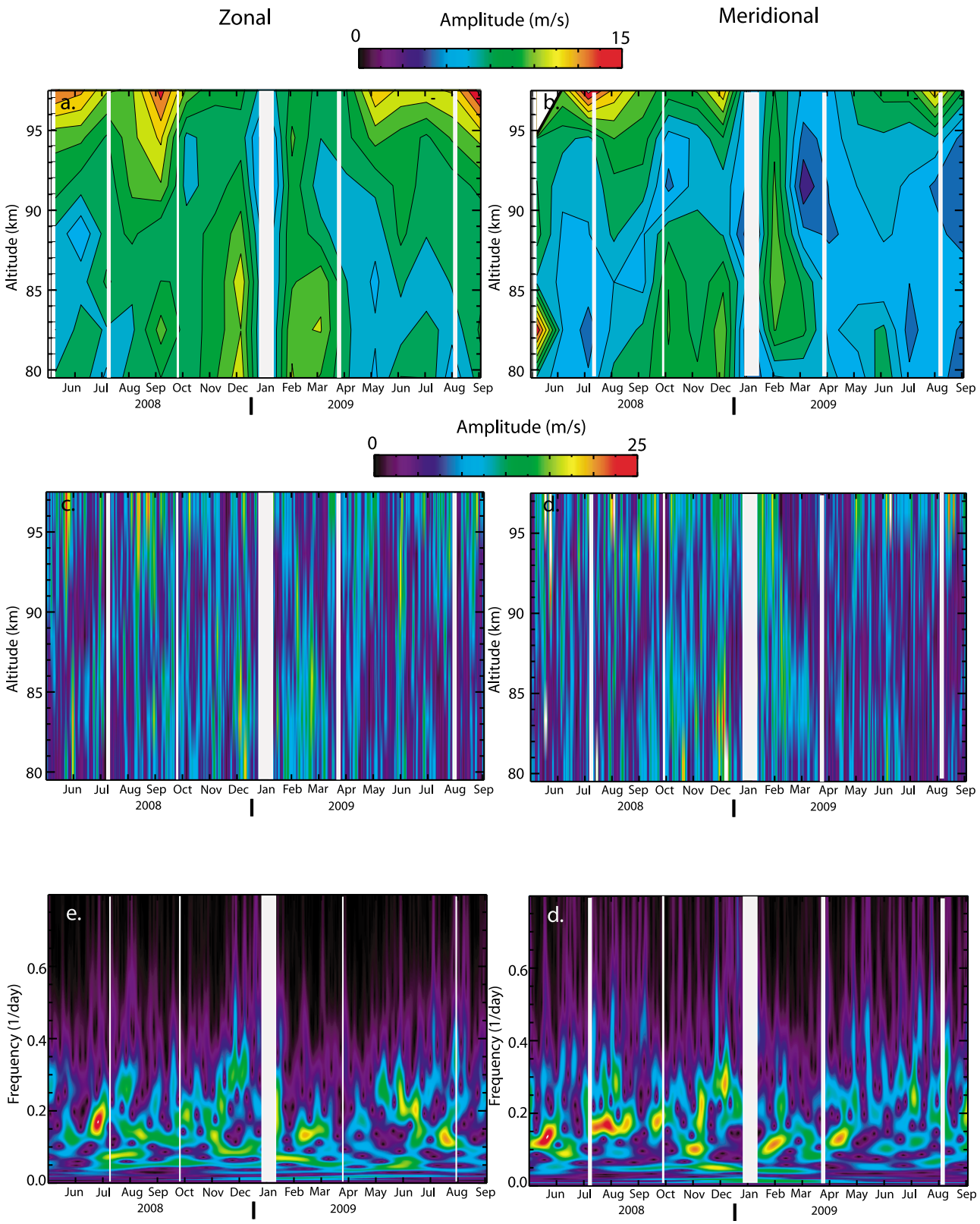

Figure 6. (top) Monthly mean diurnal tide (left) zonal and (right) meridional amplitudes, (middle) daily amplitudes, and (bottom) S transforms at 88.5 km showing the periods of tidal variability. Note the diurnal variability at ~3–30 day PW periods in both zonal and meridional components.

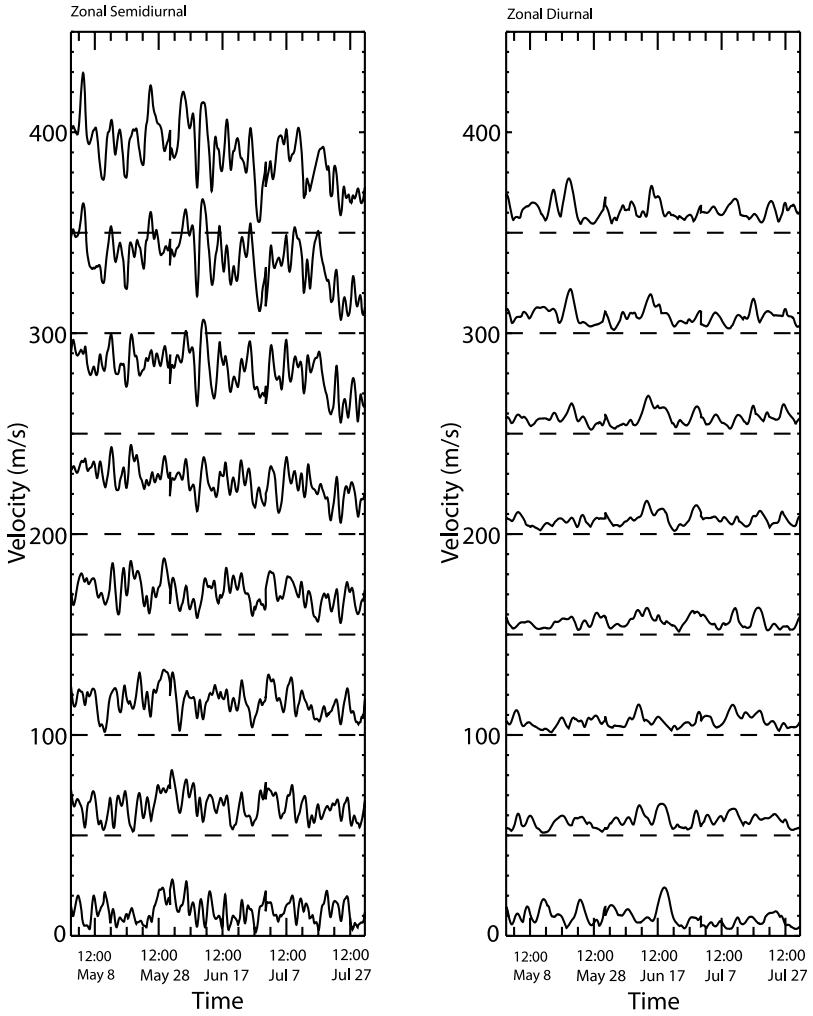

Figure 7. Daily variability of zonal (left) semidiurnal and (right) diurnal amplitudes at 3 km intervals from 76.5 to 97.5 km during May, June, and July 2009. Successive altitudes are offset by 50 m s^{-1} (dashed baselines). Diurnal amplitudes remain small at all altitudes, but semidiurnal amplitudes reach ~60–80 m s^{-1} at the highest altitudes at earlier times.

vary throughout the year. Mean diurnal amplitudes achieve maxima (>10 m s^{-1}) at higher altitudes (~95 km and above) during May, June, and September 2008 and September 2009 in the zonal components and in July and August 2008 and August of 2009 in the meridional component. Weaker maxima (typically <10 m s^{-1}) are seen at lower altitudes (below 90 km) extending from August to March but tend to be localized in altitude. We also note significant apparent interannual variability in the amplitudes observed from May to September of 2008 and 2009.

[22] Daily zonal and meridional diurnal amplitudes are displayed in the middle frames of each column in Figure 6. A subset of these data is also shown with time series of the zonal component at 3 km intervals for May, June, and July 2009 in Figure 7 (right). These exhibit much greater intermittency in time than suggested by the monthly mean amplitudes. Indeed, monthly means appear to be largely determined by infrequent events during which the diurnal tide exhibits coherence between the zonal and meridional components, but occurs with significant amplitudes for only ~1 or several days. These data also suggest modulations on various PW periods, but with little coherence in altitude, again suggesting modulations of a superposition of tidal modes comprising the overall diurnal wind field.

[23] S transforms of hourly estimates of diurnal zonal and meridional amplitudes at an altitude of 88.5 km are shown in Figure 6 (bottom). These exhibit amplitude variability on multiple PW time scales throughout the measurement period. There are a number of intervals of enhanced amplitudes exhibiting specific periodicities simultaneously in both components (see, in particular, the ~4–5 day periodicity in late November 2008 and the ~3 day periodicity in mid- to late December 2008). The large majority of significant amplitude modulations at specific PW periods, however, appear in one but not both wind components, again suggesting a superposition of modes contributing to the total diurnal fields. There is also evidence in the S transforms of gradual drifts of the modulation periods of the tidal components to shorter or longer periods that are similar to those seen in the PW amplitudes themselves. While there are some intervals during which the diurnal tide exhibits a modulation at a PW period also seen in Figure 6 (a period of ~6 days during August 2008

and periods of ~3–5 days from mid-November to late December 2008), such correlations are not frequent or robust, suggesting that any causal interactions are likely remote from our observations (also see the discussion of possible links including the semidiurnal tide below).

4.2. Semidiurnal Tide

[24] Semidiurnal tidal structures observed with SAAMER appear much less variable in altitude than the diurnal tide on monthly and daily time scales. Monthly mean and daily semidiurnal tide amplitudes are shown in the top four frames of Figure 8 and suggest generally repeatable variations from May to September of 2008 and 2009 in both components, with maximum monthly amplitudes in May and amplitudes increasing from ~15 m s^{-1} at ~80 km in both components to nearly 50 and 60 m s^{-1} (or higher) at ~98 km in the zonal and meridional components, respectively. Daily amplitudes exhibit similar altitude variations but achieve maxima that approach ~80 and 90 m s^{-1} at ~98 km in the zonal and meridional components. Weaker secondary maxima also occur in each component from August into October at ~90–98 km. A subset of these data is also shown with time series of the zonal component at 3 km intervals for May, June, and July 2009 in Figure 7 (left). As with the diurnal tide, these exhibit much greater intermittency in time than suggested by the monthly mean amplitudes. For the semidiurnal tidal components, however, there is considerably greater coherence in the short-period variations in altitude, suggesting a more consistent composition of the semidiurnal tidal structure with time than for the diurnal tide.

[25] S transforms of semidiurnal zonal and meridional amplitudes are shown in Figure 8 (bottom). As for the diurnal tide, these exhibit amplitude variability on multiple PW time scales, but the semidiurnal responses appear to be somewhat more discrete and localized in time than the diurnal responses. There are again correlations between enhanced PW responses in mean winds seen in Figure 5 and enhanced semidiurnal tide responses seen in Figure 8, for example, the ~3 day periodicity in early July 2008. However, significantly stronger correlations appear to occur between the diurnal and semidiurnal variations at various PW periods, suggesting tidal interactions modulated by PW activity that may exhibit maxima elsewhere. Examples of these correlations include the following:

[26] 1. ~6 day periodicities in August 2008 in the semidiurnal component and in late July and August 2008 in the diurnal meridional component;

[27] 2. ~6 day periodicities during October 2008 in the diurnal and semidiurnal components; and

[28] 3. ~16 day modulations of the zonal and meridional diurnal and semidiurnal components during November and early December.

[29] We also note, however, that there are other mechanisms that likely contribute to tidal modulation at various periods and that not all of these should be expected to arise from PW influences on the various tidal motions.

5. Amplitude and Phase Comparisons With GSWM-02

[30] We described the monthly mean and daily variations of the diurnal and semidiurnal tidal winds over the altitude range from 80 to 99 km in section 4. Here we focus on comparisons of monthly amplitudes and phases for each component with predictions of the GSWM-02 model at three altitudes, as an additional evaluation of GSWM-02 predictions, given that previous comparisons have revealed significant differences between observed and modeled tidal structure. Comparison altitudes were chosen to span the range of altitudes measured by SAAMER for which both measurements and GSWM-02 predictions are available. These are 82.1, 90.6, and 98.7 km for GSWM-02 at 54°S, 70°W (~150 km from SAAMER) and 81, 90, and 99 km for SAAMER. We also combined data from May to December of 2008 and 2009 to create a composite year for each field using all SAAMER data collected through 2009. These comparisons are described below. Relations to other comparisons with GSWM predictions using other data sets are discussed at the end of this section.

5.1. Diurnal Tide Comparisons

5.1.1. Annual Variations

[31] Monthly diurnal zonal and meridional amplitudes inferred from SAAMER data are shown at 81, 90, and 99 km with solid lines and open squares in Figure 9 (top). GSWM-02 predictions at altitudes of 82.1, 90.6, and 98.7 km are shown in the same frames with dashed lines and closed circles. A quick comparison of these data reveals both similarities and differences. The seasonal variability of both zonal and meridional amplitudes is surprisingly similar in the measurements and model results, including (1) double maxima in both components at ~82 km, with a secondary maximum in June in both; (2) similar seasonal cycles also extending to higher altitudes, especially in the meridional component at ~90 km and in the zonal component at ~99 km; and (3) comparable amplitude growth with altitude in both components. Differences include (1) somewhat larger amplitudes predicted by GSWM-02 than observed by SAAMER (by nearly a factor of 2) and (2) earlier maxima seen by SAAMER than in the GSWM-02 predictions in the zonal amplitudes at ~99 km.

[32] Monthly diurnal phases (defined as local time, LT, of maxima) shown in Figure 9 (bottom) likewise exhibit both strong similarities and significant differences. Phases measured by SAAMER and predicted by the GSWM-02 are remarkably similar at ~81 km, and in general agreement at ~90 km, despite the often small amplitudes of these motions. The larger differences at the lower two altitudes typically accompany the smallest measured amplitudes, where the uncertainties (vertical bars through the squares) are greatest. Despite the apparent good agreement at lower altitudes, phase measurements and predictions differ significantly at ~99 km and are more nearly in antiphase throughout the annual cycle.

[33] Relative phases of the zonal and meridional components at ~81, 90, and 99 km remain in approximate quadrature throughout the year in both SAAMER observations and GSWM-02 predictions individually, with the zonal component leading the meridional component by ~6 h, despite occasional outliers and the more nearly antiphase relation between the measurements and model results at ~99 km.

5.1.2. Altitude Variations

[34] Monthly diurnal zonal and meridional amplitudes and phases obtained from SAAMER and predicted by the GSWM-02 are shown as functions of altitude for

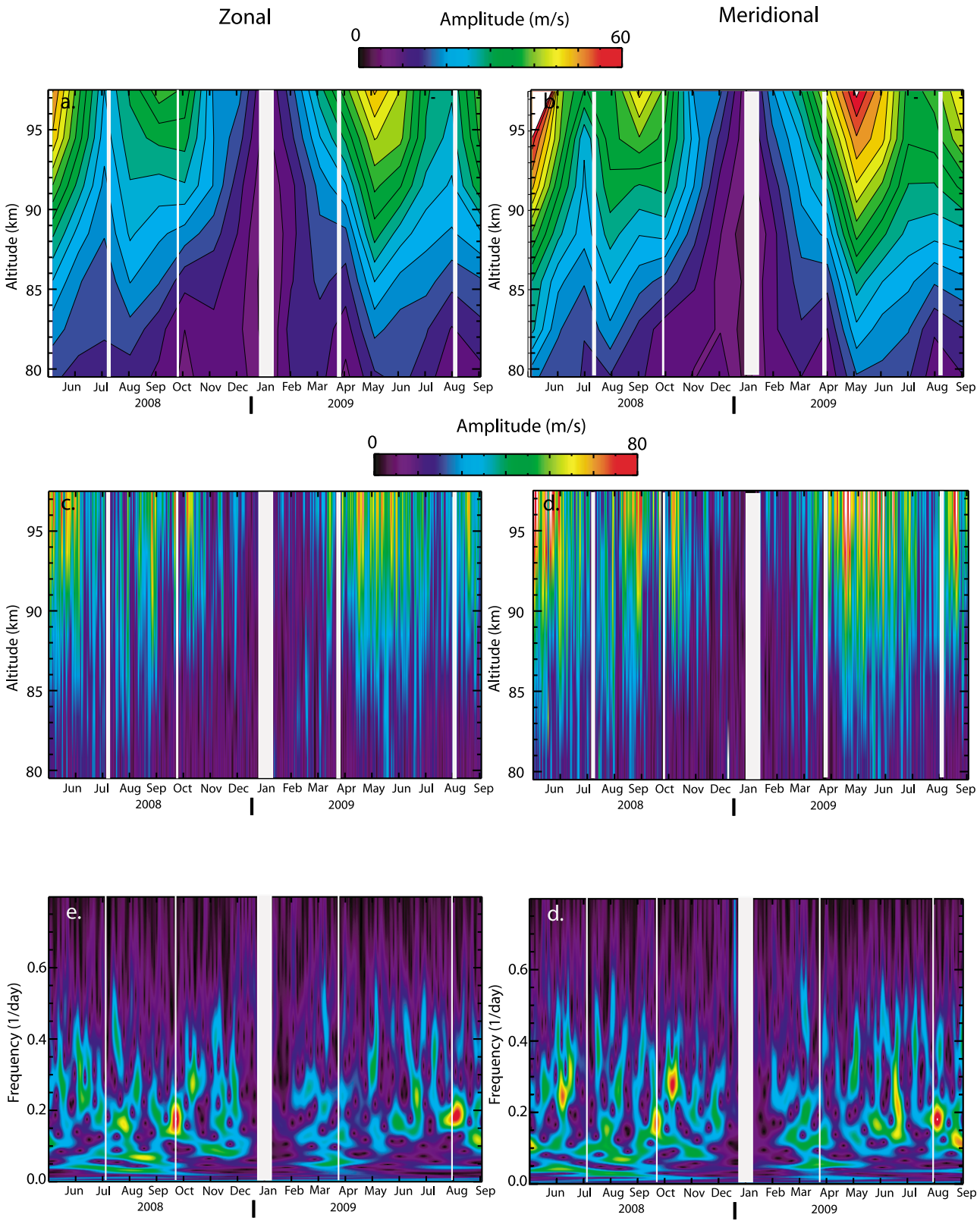

Figure 8. As in Figure 6, but for semidiurnal tide amplitudes.

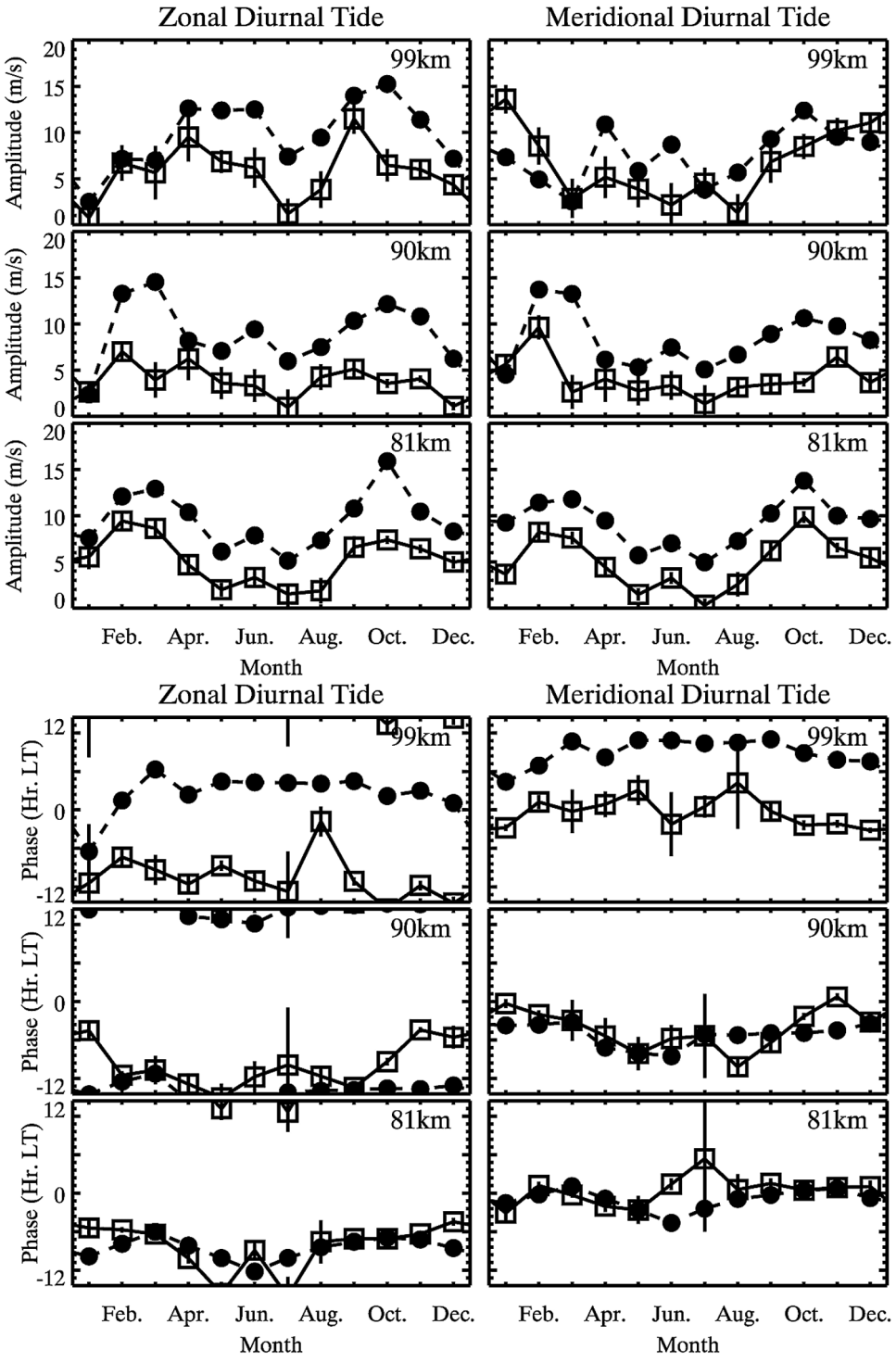

Figure 9. Monthly mean (left) zonal and (right) meridional diurnal tide amplitudes and phases (top and bottom) at 81, 90, and 99 km (bottom to top of each three frame set) from SAAMER measurements (solid lines and squares) and at 82.1, 90.6, and 98.7 km from GSWM-02 predictions (circles) from May 2008 through September 2009. SAAMER data from May through September are averages for 2008 and 2009. Uncertainties in observed amplitudes and phases are shown with error bars in each case.

March, June, September, and December in Figure 10. Here GSWM-02 predictions are shown with dashed lines and closed circles and SAAMER data are shown with solid lines and diamonds (2008) or triangles (2009). As seen in Figure 9, GSWM-02 amplitudes are comparable to, or larger than, those observed by SAAMER, except in December above ~90 km. Amplitudes are also quite variable with altitude, with both SAAMER measurements and GSWM-02 predictions

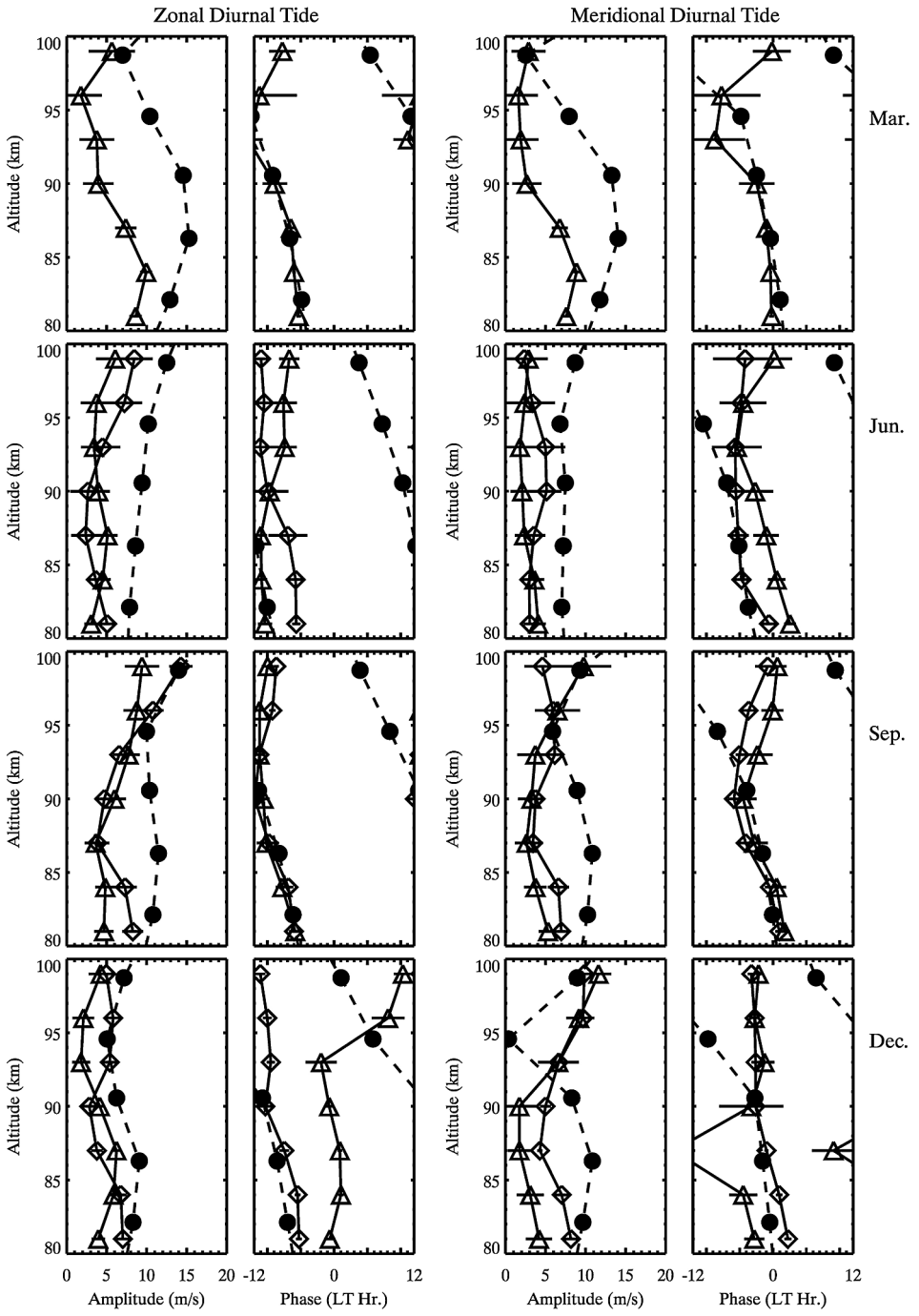

Figure 10. Vertical profiles of monthly mean (left) zonal and (right) meridional diurnal tide amplitudes and phases (left and right within each column) from 81 to 99 km for March, June, September, and December (solid lines, with diamonds for 2008 and triangles for 2009). GSWM02 predictions are shown with dashed lines and circles for comparison, and uncertainties are shown with error bars in each case.

exhibiting both increasing and decreasing amplitudes between 81 and 99 km in each of the profiles. The general interannual agreement of the amplitude profiles in both wind components during June and September, for which SAAMER data are available for 2008 and 2009, also suggests confidence in these estimates and some consistency in the diurnal modes comprising these mean responses each year. These data also suggest that the approximate quadrature between the zonal and meridional components noted above appears to be preserved over the full altitude range.

[35] In contrast to the tidal amplitude variations, mean diurnal zonal and meridional phases for these 4 months agree extremely well up to ~90 km, with phase differences of a few hours between 2008 and 2009 in each component only occurring during June. Above 90 km, however, SAAMER LT maxima either increase, are nearly constant, or decrease

weakly with altitude, while GSWM-02 LT maxima decrease sharply in both components in all 4 months by ~5–12 h over an altitude of only ~8 km.

[36] Collectively, these results suggest that the GSWM-02 provides a description of the diurnal tidal structures at this latitude and longitude that are (1) a slight overestimate of tidal amplitudes, with somewhat better agreement at the highest altitudes; (2) a very accurate estimate of phase up to ~90 km; and (3) a sharp departure from observed phase structures above ~90 km.

5.2. Semidiurnal Tide Comparisons

5.2.1. Annual Variations

[37] Monthly semidiurnal zonal and meridional amplitudes inferred from SAAMER data are shown at 81, 90, and 99 km with solid lines and open squares in Figure 11 (top). GSWM-02 predictions at altitudes of 82.1, 90.6, and 98.7 km are shown in the same frames with dashed lines and closed circles. As in the diurnal comparisons, there are both similarities and differences in these distributions. Annual variations in amplitudes in both SAAMER observations and the GSWM-02 exhibit broad winter maxima extending from about February or March to about September or October, with the earlier autumn starts occurring at lower altitudes in SAAMER data and later spring cessations occurring at middle and higher altitudes (~90 and 99 km) in both SAAMER data and GSWM-02 predictions. Amplitudes in both SAAMER data and GSWM-02 predictions increase significantly with altitude, are slightly larger for the meridional than for the zonal component at all altitudes, and develop double maxima in May and September at the highest altitudes. Unlike the diurnal wind components, however, GSWM-02 predictions of semidiurnal amplitudes are systematically smaller than SAAMER observations at lower and middle altitudes (~81 and 90 km) and only become comparable or larger at ~99 km during July, August, and September. Whereas SAAMER diurnal amplitudes are typically ~10 m s^{-1} or less at all altitudes (except for the zonal component in September of ~12 m s^{-1} and the meridional component in January of ~14 m s^{-1}), maximum semidiurnal amplitudes increase from ~15–20 m s^{-1} at 81 km to ~50–60 m s^{-1} at 99 km.

[38] Phases (defined as LTs of maximum amplitudes) of the monthly mean semidiurnal zonal and meridional winds are shown in Figure 11 (bottom). The overall agreement between SAAMER observations and GSWM-02 predictions is quite good, especially at the highest altitudes, where the phases nearly overlay each other and differ by only ~1 h where amplitudes are large and ~2 h where amplitudes are smallest. Similar agreement is seen at ~90 km where amplitudes are ~20 m s^{-1} or larger and at ~81 km where amplitudes are ~15 m s^{-1} or larger. Where amplitudes are smaller than ~5 m s^{-1}, GSWM-02 phase predictions are most often advanced relative to SAAMER observations by ~2–5 h, with a single value at 81 km in December advanced by more than 8 h. As seen in the diurnal phases, the zonal and meridional components are nearly in quadrature, with the meridional component leading the zonal component by ~3 h during most months at all three altitudes displayed.

5.2.2. Altitude Variations

[39] Monthly semidiurnal zonal and meridional amplitudes and phases obtained from SAAMER and predicted by the GSWM-02 as functions of altitude for March, June, September, and December are shown in Figure 12. As in Figure 10, GSWM-02 predictions are shown with dashed lines and closed circles and SAAMER data are shown with solid lines and diamonds (2008) or triangles (2009). Where and when amplitudes are small, i.e., at the lowest altitudes and during March and December, GSWM-02 amplitudes are comparable to or smaller than those measured by SAAMER, typically a factor of ~2 smaller at altitudes above ~90 km. GSWM-02 amplitudes are also systematically smaller than SAAMER amplitudes at all altitudes during June, where maximum SAAMER amplitudes are ~40–50 m s^{-1} at ~99 km. Only during September do GSWM-02 amplitudes become large and comparable to SAAMER amplitudes, even slightly exceeding them at ~99 km, with maxima of ~45 m s^{-1} where SAAMER amplitudes are ~30–40 m s^{-1}. As seen above for the diurnal tide, SAAMER data for June and September during 2008 and 2009 exhibit good agreement in amplitude and phase, suggesting high confidence in our general amplitude and phase estimates.

[40] Comparing monthly semidiurnal phases, we see that SAAMER measurements and GSWM-02 predictions are in very good agreement, within ~1 h, for June and September above ~85 km where amplitudes are large. During March and December, where SAAMER and GSWM-02 amplitudes are smaller, ~3–20 m s^{-1}, phase differences are larger, with GSWM-02 leading SAAMER by ~4 h at ~88 km and ~1 h at ~99 km. At lower altitudes during March, phases agree well, despite amplitudes of only ~5–10 m s^{-1}, but differ significantly in December where both SAAMER and GSWM-02 amplitudes are <5 m s^{-1}. As noted above, the semidiurnal zonal and meridional winds are in approximate quadrature wherever amplitudes are sufficiently large to permit confident phase determinations.

5.3. Comparisons With Other Data Sets

[41] Intercomparisons of tidal observations with predictions of the GSWM model have been reported by a number of authors employing various data sets. Our purpose here is to review these previous comparisons in light of our own discussed above.

5.3.1. Diurnal Tide Comparisons

[42] Comparisons of extensive radar measurements during the June–August 1999 PSMOS campaign with GSWM predictions by *Pancheva et al.* [2002] revealed larger diurnal phase variations at southern than at northern latitudes and significant departures from GSWM predictions, especially at higher altitudes. More focused studies by *Vincent et al.* [1998] and *Tomikawa and Tsutsumi* [2009] noted significant phase departures at higher altitudes due to the smaller vertical wavelengths predicted by an earlier version of the GSWM. Lidar measurements at Fort Collins [*Yuan et al.*, 2006] also revealed an overestimate of diurnal amplitudes predicted by GSWM-02 compared to observations at that site. These departures are all consistent with our own observations at higher southern latitudes (see Figure 10) and their departures from predictions of GSWM-02.

[43] The study of the diurnal tide by *Pancheva et al.* [2009] employing TIMED/SABER temperature measurements at 90 km revealed a primary maximum in February and a secondary maximum in September, in reasonable agreement with our own observations (see Figure 9), though SAAMER maxima occur somewhat later at lower and higher altitudes.

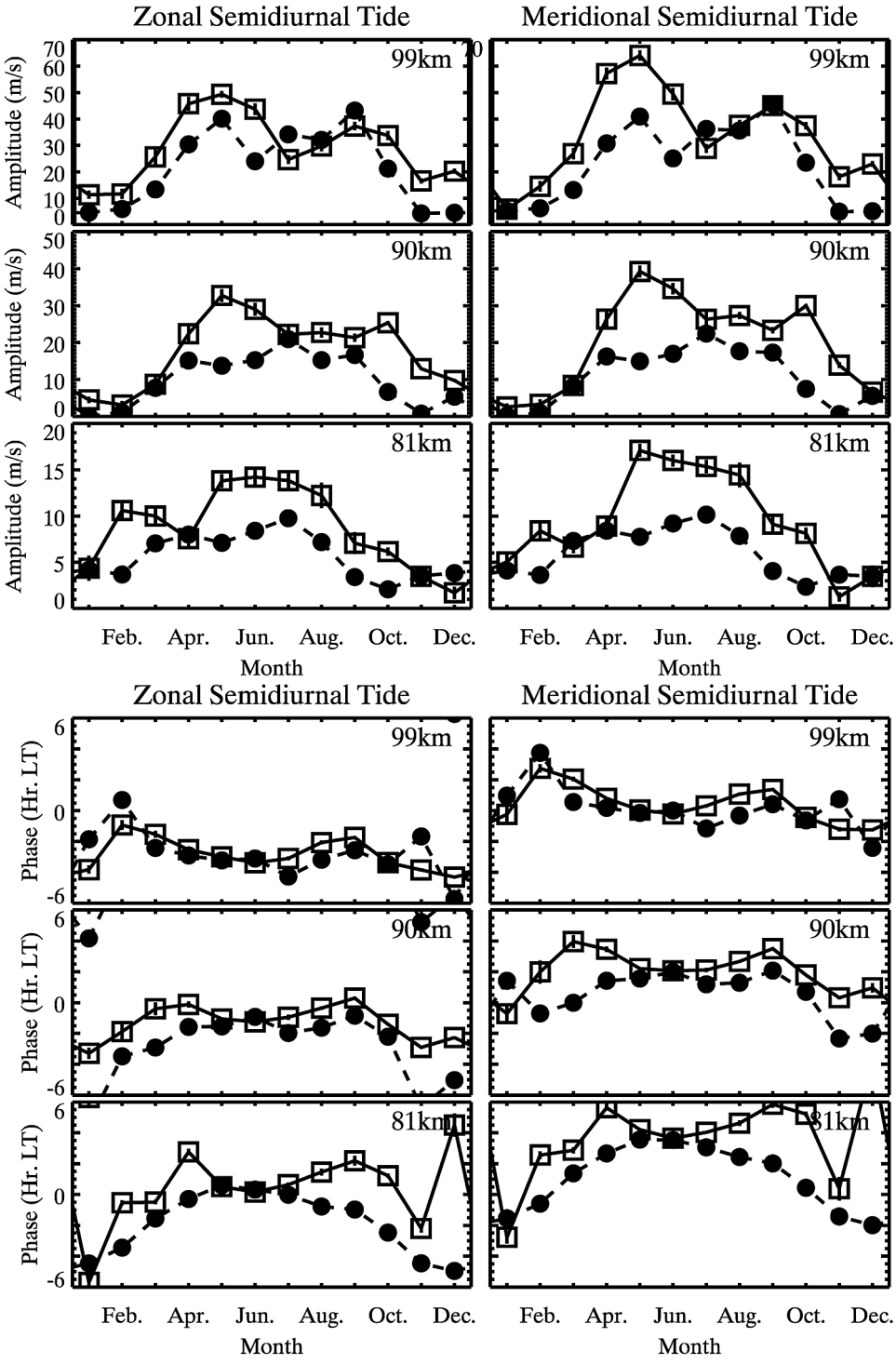

Figure 11. As in Figure 9, but for the semidiurnal tide.

SAAMER diurnal phases are somewhat more variable than inferred from SABER data, perhaps because SAAMER measurements also include influences of the nonmigrating diurnal components. Nonmigrating diurnal components were also studied by *Oberheide et al.* [2006] employing TIMED/TIDI wind measurements, but these do not seem pertinent to our discussion as SAAMER cannot distinguish between the migrating and nonmigrating contributions by itself.

5.3.2. Semidiurnal Tide Comparisons

[44] A number of previous studies compared radar or optical measurements of semidiurnal tides at high northern and southern latitudes with predictions of the GSWM. Fabry-Perot interferometer (FPI) measurements by *Fisher et al.* [2002] revealed much longer vertical wavelengths (~90 km) from December to February than predicted by the GSWM (~40 km). The study by *Murphy et al.* [2003] found the phase structure of the migrating semidiurnal tide to agree well with

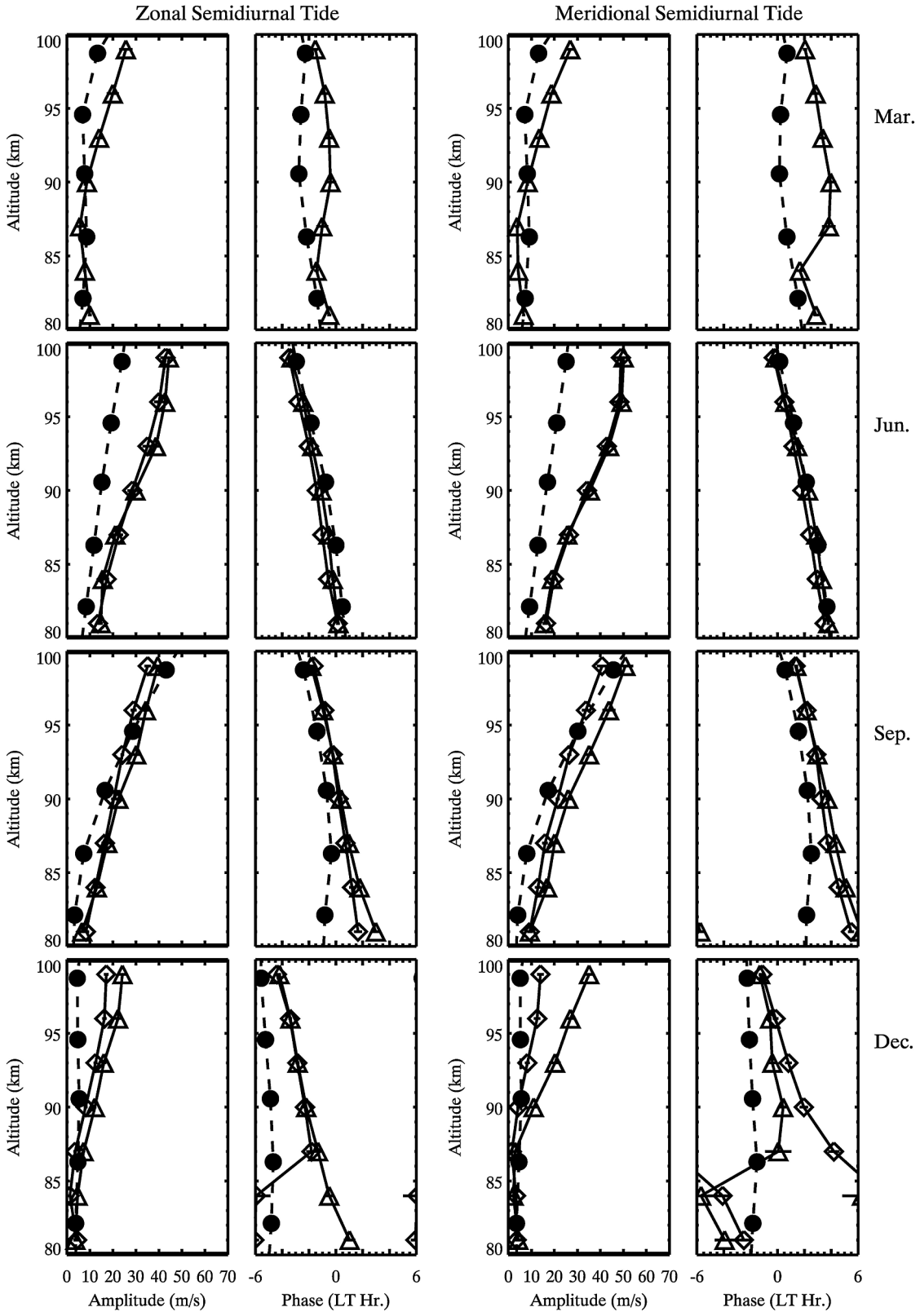

Figure 12. As in Figure 10, but for the semidiurnal tide.

GSWM predictions during austral winter but to depart significantly during austral summer. Similar results were also obtained by *Mitchell et al.* [2002] employing radar measurements at an arctic site. Finally, an analysis of TIMED/SABER temperature data at 90 km by *Mukhtarov et al.* [2009] found a primary amplitude maximum during May at 40°S that corresponds closely to that seen by SAAMER at 90 km but with closer agreement with the occurrence of a secondary maximum in SAAMER data (and with the prediction of both maxima by GSWM) at ~99 km.

6. Summary and Conclusions

[45] We described in this paper a new meteor radar, the Southern Argentina Agile Meteor Radar (SAAMER), which was specifically designed to provide very high resolution wind measurements for assessments of mean, PW, and tidal wind fields, a potential for assessing GW momentum fluxes, and advanced meteor studies. We also described the mean and tidal wind fields throughout the first ~16 months of SAAMER operations, their variations on seasonal and PW time scales and with altitude, and comparisons of SAAMER monthly mean diurnal and semidiurnal tidal wind measurements with predictions of the GSWM-02.

[46] SAAMER employs a transmitter with 60 kW peak power and a circular transmitting antenna array composed of eight three-element crossed yagis having opposite phasing of every other yagi to define a beam pattern having eight beams with peak sensitivity at ~35° zenith angles. Our initial studies employed a single 13 μs pulse (yielding a 2 km range bin), a pulse repetition frequency of 2144 Hz, an integration over four samples, and yielded ~12,000 accepted meteor detections per day. However, the SAAMER sampling mode was changed to a two-baud code in September 2009 that yields an ~50% increase in accepted meteor counts.

[47] Measurements from May 2008 to September 2009 reveal monthly mean zonal winds (1) that are eastward for most of the year, except from about mid-October to late February at ~80 km and from mid-November to mid-December at ~90 km, (2) having eastward maxima occurring from about February to August above ~85 km of ~45 m s^{-1}, and (3) having a westward maximum extending from mid-November into late December with a magnitude of ~45 m s^{-1}. Monthly mean meridional winds are primarily northward from mid-October to mid-March at all altitudes, with maxima of ~15 m s^{-1}. From mid-October to mid-March, however, monthly mean winds are primarily southward, but exhibit very significant variability on ~60–90 day periods, with northward maxima centered near 90 km during December 2008 and at ~80–85 km during February 2009 and ~85–95 km during July and September 2009.

[48] Daily mean winds exhibit considerably more variability and highlight the PW influences where they occur most strongly. PWs make relatively greater contributions to daily mean winds from about February to September and contribute much less when monthly mean winds are westward. They also contribute much greater variability in the zonal than in the meridional wind field. For most of the year, however, PWs are seen to make major contributions to the monthly mean winds, either positive or negative, and to their apparent variability on longer time scales.

[49] Tidal winds, especially the semidiurnal tide, contribute very significantly to the motion field over SAAMER. Semidiurnal zonal and meridional amplitudes achieve monthly mean maxima approaching ~50 and 60 m s^{-1}, respectively, above 95 km in May, with large amplitudes extending from April into June and secondary, weaker maxima extending from August to October. At these times, the semidiurnal tide also grows strongly with altitude. Monthly mean diurnal amplitudes are significantly weaker, ~10–15 m s^{-1}, and vary considerably in altitude and time. Both the semidiurnal and diurnal tides also exhibit significant short-term variability, with the daily semidiurnal zonal and meridional components achieving daily maxima of ~80 and 90 m s^{-1} and the daily diurnal components achieving maxima ~20 and 25 m s^{-1}, respectively. Both the diurnal and semidiurnal tides also exhibit significant variability on PW periods ranging from ~3 to 30 days, with clear correlations between occurrences of PW activity at specific periods and tidal modulations at the same periods.

[50] Comparisons of SAAMER monthly mean tidal amplitudes and phases with predictions of these fields by the GSWM-02 (~150 km from SAAMER) reveal that the GSWM-02 generally predicts diurnal wind amplitudes for all altitudes from ~82 to 98 km that are larger than observed, with the largest fractional differences at the lowest altitudes. Despite this, GSWM-02 does reasonably well in defining the annual cycle of monthly mean amplitudes, especially at the lower altitudes and in the meridional component. GSWM-02 phase predictions are in very reasonable agreement with observations at lower and middle altitudes (~82–91 km) where amplitudes are sufficiently large to determine phases with confidence. GSWM-02 phase predictions differ very significantly from SAAMER observations at the highest altitudes, however, with GSWM-02 phases leading SAAMER phases by ~6–10 h in both components for most of the annual cycle. All of the major differences occur at the highest altitudes, where GSWM-02 phases decrease sharply with altitude (toward earlier LTs of maxima) while SAAMER observations suggest phases are constant or increasing with altitude above ~90 km.

[51] Comparisons of semidiurnal amplitudes and phases reveal that GSWM-02 typically underpredicts semidiurnal amplitudes for all altitudes measured by SAAMER. Where SAAMER measures monthly mean semidiurnal zonal and meridional wind amplitudes having maximum values varying from ~15–18 m s^{-1} at ~82 km to ~50–60 m s^{-1} at ~98 km, respectively, GSWM-02 instead predicts amplitudes of ~10 m s^{-1} or less at ~82 km increasing to ~40–50 m s^{-1} at ~98 km. Seasonal variations of amplitudes agree somewhat between SAAMER and GSWM-02 at the lowest and highest altitudes, but with GSWM-02 underestimating the winter amplitude maximum at ~82 km and suggesting larger amplitudes in September than from April to June at ~98 km in contrast to SAAMER measurements. GSWM-02 also fails to describe the broad maximum extending from April to October with a May–June maximum at ~91 km. GSWM-02 and SAAMER phase estimates are nevertheless in close agreement where amplitudes are significant, and especially at middle and higher altitudes. GSWM-02 and SAAMER phase variations with altitude for the semidiurnal tide agree very closely where amplitudes are sufficient to allow confident

estimates. Finally, monthly mean diurnal and semidiurnal amplitudes and phases inferred with SAAMER are very consistent for those months for which measurements are available in both 2008 and 2009, suggesting high confidence in the ability to define these tidal fields well with SAAMER.

[52] Previous comparisons of radar tidal measurements with GSWM-02 predictions have been confined to Antarctic latitudes [*Murphy et al.*, 2003, 2006; *Hibbins et al.*, 2006; *Tomikawa and Tsutsumi*, 2009]. Very reasonable agreement was observed in specific cases, in particular the westward-propagating wave number 2 semidiurnal tidal phase from May to September [*Murphy et al.*, 2003, 2006] and the seasonal variations of the migrating diurnal tidal amplitude and its phase variations with altitude in austral summer [*Tomikawa and Tsutsumi*, 2009]. The majority of such comparisons suggest, however, that nonlinear interactions play a critical role in the excitation of nonmigrating tidal modes, especially the westward-propagating wave number 1 component, and that the inability of GSWM-02 to describe these modes leads, in part, to its incomplete characterization of the overall tidal structures at high latitudes.

[53] We conclude that SAAMER performs as hoped for measurements of the large-scale mean, tidal, and PW winds. Tidal measurements also indicate systematic differences from GSWM-02 that suggest additional dynamical influences (sources, interactions, filtering, or dissipation processes) are required to quantitatively describe the tidal fields at these altitudes.

[54] **Acknowledgments.** The acquisition and installation of the SAAMER radar and the research described in this paper were performed under NSF grants ATM-0634650 and ATM-0824742. We are especially grateful to MARDOC and Genesis Software for working with us to devise a radar hardware and antenna configuration that met our measurement objectives. We also acknowledge use of the CEDAR data base and the GSWM-02 Web site at National Center for Atmospheric Research (NCAR) for GSWM-02 results employed for our comparisons.

References

Alexander, M. J., et al. (2008a), Global estimates of gravity wave momentum flux from High Resolution Dynamics Limb Sounder observations, *J. Geophys. Res.*, *113*, D15S18, doi:10.1029/2007JD008807.

Alexander, M. J., H. Teitelbaum, S. D. Eckermann, J. Gille, J. Barnett, and C. Barnet (2008b), High-resolution satellite observations of mountain waves, *Bull. Am. Meteorol. Soc.*, *89*, 151–152.

Avery, S. K., R. A. Vincent, A. Phillips, A. H. Manson, and G. J. Fraser (1989), High-latitude tidal behavior in the mesosphere and lower thermosphere, *J. Atmos. Terr. Phys.*, *51*(7/8), 595–608.

Baumgaertner, A. J. G., A. J. McDonald, R. E. Hibbins, D. C. Fritts, D. J. Murphy, and R. A. Vincent (2008), Short-period planetary waves in the Antarctic middle atmosphere, *J. Atmos. Sol.-Terr. Phys.*, *70*(10), 1336–1360.

Burrage, M. D., M. E. Hagan, W. R. Skinner, D. L. Wu, and P. B. Hays (1995), Long-term variability in the solar diurnal tide observed by HRDI and simulated by the GSWM, *Geophys. Res. Lett.*, *22*(19), 2641–2644.

Dowdy, A. J., R. A. Vincent, M. Tsutsumi, K. Igarashi, Y. Murayama, W. Singer, and D. J. Murphy (2007), Polar mesosphere and lower thermosphere dynamics: 1. Mean wind and gravity wave climatologies, *J. Geophys. Res.*, *112*, D17104, doi:10.1029/2006JD008126.

Eckermann, S. D., et al. (2006), Imaging gravity waves in lower stratospheric AMSU-A radiances, Part 2: Validation case study, *Atmos. Chem. Phys.*, *6*, 3343–3362.

Ern, M., P. Preusse, M. J. Alexander, and C. D. Warner (2004), Absolute values of gravity wave momentum flux derived from satellite data, *J. Geophys. Res.*, *109*, D20103, doi:10.1029/2004JD004752.

Espy, P. J., G. O. L. Jones, G. R. Swenson, J. Tang, and M. J. Taylor (2004), Tidal modulation of the gravity-wave momentum flux in the Antarctic mesosphere, *Geophys. Res. Lett.*, *31*, L11111, doi:10.1029/2004GL019624.

Espy, P. J., R. E. Hibbins, G. R. Swenson, J. Tang, M. J. Taylor, D. M. Riggin, and D. C. Fritts (2006), Regional variations of mesospheric gravity wave momentum fluxes over Antarctica, *Ann. Geophys.*, *24*, 81–88, SRef-ID: 1432-0576/ag/2006-24-81.

Fisher, G. M., R. J. Niciejewski, T. L. Killeen, W. A. Gault, G. G. Shepherd, S. Brown, and Q. Wu (2002), Twelve-hour tide in the winter northern polar mesosphere and lower thermosphere, *J. Geophys. Res.*, *107*(A8), 1211, doi:10.1029/2001JA000294.

Forbes, J. M., J. Gu, and S. Miyahara (1991), On the interactions between gravity waves and the diurnal propagating tide, *Planet. Space Sci.*, *39*, 1249–1257.

Fritts, D. C., and R. A. Vincent (1987), Mesospheric momentum flux studies at Adelaide, Australia: Observations and a gravity wave/tidal interaction model, *J. Atmos. Sci.*, *44*, 605–619.

Fritts, D. C., and M. J. Alexander (2003), Gravity wave dynamics and effects in the middle atmosphere, *Rev. Geophys.*, *41*(1), 1003, doi:10.1029/2001RG000106.

Fritts, D. C., T. Tsuda, T. E. VanZandt, S. A. Smith, T. Sato, S. Fukao, and S. Kato (1990), Studies of velocity fluctuations in the lower atmosphere using the MU radar: II. Momentum fluxes and energy densities, *J. Atmos. Sci.*, *47*, 51–66.

Fritts, D. C., D. Janches, and W. K. Hocking (2010), Southern Argentina Agile Meteor Radar (SAAMER): Initial assessment of gravity wave momentum fluxes, *J. Geophys. Res.*, doi:10.1029/2010JD013891, in press.

Guest, F. M., M. J. Reeder, C. J. Marks, and D. J. Karoly (2000), Inertia-gravity waves observed in the lower stratosphere over Macquarie Island, *J. Atmos. Sci.*, *57*, 737–752.

Hagan, M. E., and J. M. Forbes (2002), Migrating and nonmigrating diurnal tides in the middle and upper atmosphere excited by tropospheric latent heat release, *J. Geophys. Res.*, *107*(D24), 4754, doi:10.1029/2001JD001236.

Hagan, M. E., and J. M. Forbes (2003), Migrating and nonmigrating semidiurnal tides in the upper atmosphere excited by tropospheric latent heat release, *J. Geophys. Res.*, *108*(A2), 1062, doi:10.1029/2002JA009466.

Hagan, M. E., M. D. Burrage, J. M. Forbes, J. Hackney, W. J. Randel, and X. Zhang (1999), GSWM-98: Results for migrating solar tides, *J. Geophys. Res.*, *104*(A4), 6813–6827.

Hertzog, A., G. Boccara, R. A. Vincent, F. Vial, and P. Cocquerez (2008), Estimation of gravity wave momentum flux and phase speeds from quasi-Lagrangian stratospheric balloon flights. Part II: Results from the Vorcore campaign in Antarctica, *J. Atmos. Sci.*, *65*, 3056–3070.

Hibbins, R. E., P. J. Espy, and M. J. Jarvis (2006), Mean winds and tides in the mesosphere and lower thermosphere above Halley, Antarctica., *J. Atmos. Sol.-Terr. Phys.*, *68*, 436–444.

Holton, J. R. (1984), The generation of mesospheric planetary waves by zonally asymmetric gravity wave breaking, *J. Atmos. Sci.*, *41*, 3427–3430.

Isler, J. R., and D. C. Fritts (1996), Gravity wave variability and interactions with lower-frequency motions in the mesosphere and lower thermosphere over Hawaii, *J. Atmos. Sci.*, *53*, 37–48.

Janches, D., S. Palo, E. M. Lau, S. K. Avery, J. P. Avery. S. de la Peña, and N. A. Makarov (2004), Diurnal and seasonal variability of the meteor flux at the South Pole measured with radars, *Geophys. Res. Lett.*, *31*, L20807, doi:10.1029/2004GL021104.

Janches, D., C. J. Heinselman, J. L. Chau, A. Chandran, and R. Woodman (2006), Modeling the micrometeor input function in the upper atmosphere observed by high power and large aperture radars, *111*, A07317, doi:10.1029/2006JA011628.

Jiang, J. H., D. L. Wu, and S. D. Eckermann (2002), Upper Atmosphere Research Satellite (UARS) MLS observation of mountain waves over the Andes, *J. Geophys. Res.*, *107*(D20), 8273, doi:10.1029/2002JD002091.

Jiang, J. H., S. D. Eckermann, D. L. Wu, and D. Y. Wang (2006), Interannual variation of gravity waves in the Arctic and Antarctic winter middle atmosphere, *Adv. Space Res.*, *37*, 2418–2423.

Lu, W., and D. C. Fritts (1993), Spectral estimates of gravity wave energy and momentum fluxes, III: Gravity wave-tidal interactions, *J. Atmos. Sci.*, *50*, 3714–3727.

Manson, A. H., C. E. Meek, and G. E. Hall (1998), Correlations of gravity waves and tides in the mesosphere over Saskatoon, *J. Atmos. Sol.-Terr. Phys.*, *60*, 1089–1107.

Manson, A. H., et al. (1999), Seasonal variations of the semidiurnal and diurnal tides in the MLT: multiyear MF radar observations from 2 to 70°N, and the GSWM tidal model, *J. Atmos. Sol.-Terr. Phys.*, *61*(11), 809–828, doi:10.1016/S1364-6826(99)00045-0.

McLandress, C. (1998), On the importance of gravity waves in the middle atmosphere and their parameterization in general circulation models, *J. Atmos. Sol.-Terr. Phys.*, *60*, 1357–1383.

McLandress, C. (2002), The seasonal variation of the propagating diurnal tide in the mesosphere and lower thermosphere. Part I: The role of gravity waves and planetary waves, *J. Atmos. Sci.*, *59*(5), 907–922.

McLandress, C., and W. E. Ward (1994), Tidal/gravity wave interactions and their influence on the large-scale dynamics of the middle atmosphere: Model results, *J. Geophys. Res.*, *99*, 8139–8156.

McLandress, C., M. J. Alexander, and D. L. Wu (2000), Microwave Limb Sounder observations of gravity waves in the stratosphere: A climatology and interpretation, *J. Geophys. Res.*, *105*(D9), 11,947–11,967.

Meyer, C. K. (1999), Gravity wave interactions with the diurnal propagating tide, *J. Geophys. Res.*, *104*, 4223–4239.

Mitchell, N. J., D. Pancheva, and H. R. Middleton (2002), Mean winds and tides in the Arctic mesosphere and lower thermosphere, *J. Geophys. Res.*, *107*(A1), 1004, doi:10.1029/2001JA900127.

Miyahara, S. (1985), Suppression of stationary planetary waves by internal gravity waves in the mesosphere, *J. Atmos. Sci.*, *42*, 100–107.

Miyahara, S., Y. Hayashi, and J. D. Mahlman (1986), Interactions between gravity waves and planetary-scale flow simulated by the GFDL "SKYHI" general circulation model, *J. Atmos. Sci.*, *43*, 1844–1861.

Mukhtarov, P., D. Pancheva, and B. Andonov (2009), Global structure and seasonal and interannual variability of the migrating diurnal tide seen in the SABER/TIMED temperatures between 20 and 1290 km, *J. Geophys. Res.*, *114*, A02309, doi:10.1029/2008JA013759.

Murphy, D. J., and R. A. Vincent (1998), Mesospheric momentum fluxes over Adelaide during the 2 day wave: Results and interpretation, *J. Geophys. Res.*, *103*, 28,627–28,636.

Murphy, D. J., M. Tsutsumi, D. M. Riggin, G. O. L. Jones, R. A. Vincent, M. E. Hagan, and S. K. Avery (2003), Observations of a nonmigrating component of the semidiurnal tide over Antarctica., *J. Geophys. Res.*, *108*(D8), 4241, doi:10.1029/2002JD003077.

Murphy, D. J., et al. (2006), A climatology of tides in the Antarctic mesosphere and lower thermosphere, *J. Geophys. Res.*, *111*, D23104, doi:10.1029/2005JD006803.

Murphy, D. J., W. J. R. French, and R. A. Vincent (2007), Long-period planetary waves in the mesosphere and lower thermosphere above Davis, Antarctica, *J. Atmos. Sol.-Terr. Phys.*, *69*, doi:10.1016/j.jastp.2007.06.008, 2118–2138.

Oberheide, J., Q. Wu, T. L. Killeen, M. E. Hagan, and R. G. Roble (2006), Diurnal nonmigrating tides from TIDI wind data: Monthly climatologies and seasonal variations, *J. Geophys. Res.*, *111*, A10S03, doi:10.1029/2005JA011491.

Pancheva, D., et al. (2002), Global-scale tidal structure in the mesosphere and lower-thermosphere during the PSMOS campaign of June-August 1999 and comparisons with the global-scale wave model, *J. Atmos. Sol.-Terr. Phys.*, *64*, 1011–1035.

Pancheva, D., et al. (2004), Variability of the quasi-2 day wave observed in the MLT region during the PSMOS campaign of June–August 1999, *J. Atmos. Sol.-Terr. Phys.*, *66*, doi:10.1016/j.jastp.2004.01.008, 539–565.

Pancheva, D. V., et al. (2006), Two-day wave coupling of the low-latitude atmosphere-ionosphere system, *J. Geophys. Res.*, *111*, A07313, doi:10.1029/2005JA011562.

Pancheva, D., P. Mukhtarov, and B. Andonov (2009), Global structure, seasonal and interannual variability of the migrating semidiurnal tide seen in the SABER/TIMED temperatures (2002–2007), *Ann. Geophys.*, *27*, 687–703.

Portnyagin, Y., et al. (2004), Mesosphere/lower thermosphere prevailing wind model, *Adv. Space Res.*, *34*, 1755–1762.

Portnyagin, Y. I., E. G. Merzlyakov, T. V. Solov'eva, and N. A. Makarov (2006), Interhemispheric distinctions in wind-regime parameters in the polar mesosphere-lower thermosphere, Izvestiya, *Atmos. Oceanic. Phys.*, *42*(1), 93–104.

Preusse, P., A. Dornbrack, S. D. Eckermann, M. Riese, B. Schaeler, J. T. Bacmeister, D. Broutman, and K. U. Grossmann (2002), Space based measurements of stratospheric mountain waves by CRISTA, 1. Sensitivity, analysis method and a case study, *J. Geophys. Res.*, *107*(D23), 8178, doi:10.1029/2001JD000699.

Preusse, P., M. Ern, S. D. Eckermann, C. D. Warner, R. H. Picard, P. Knieling, M. Krebsbach, J. M. Russell III, M. G. Mlynczak, C. J. Mertens, and M. Riese (2006), Tropopause to mesopause gravity waves in August: Measurement and modeling, *J. Atmos. Sol.-Terr. Phys.*, *68*, 1730–1751.

Smith, S., J. Baumgardner, and M. Mendillo (2009), Evidence of mesospheric gravity-waves generated by orographic forcing in the troposphere, *Geophys. Res. Lett.*, *36*, L08807, doi:10.1029/2008GL036936.

Stockwell, R. G., L. Mansinha, and R. Lowe (1996), Localization of the complex spectrum: The S transform, *IEEE Trans. Signal Process.*, *44*(4), 998–1001.

Thayaparan, T., W. K. Hocking, and J. MacDougall (1995), Observational evidence of tidal/gravity wave interactions using the UWO 2MHz radar, *Geophys. Res. Lett.*, *22*, 373–376.

Tomikawa, Y., and M. Tsutsumi (2009), MF radar observations of the diurnal tide over Syowa, Antarctica (69o S, 40o E), *Ann. Geophys.*, *27*, 2653–2659.

Tsuda, T., M. Nishida, C. Rocken, and R. H. Ware (2000), A global morphology of gravity wave activity in the stratosphere revealed by the GPS occultation data GPS/MET, *J. Geophys. Res.*, *105*, 7257–7273.

VanZandt, T. E., S. A. Smith, T. Tsuda, D. C. Fritts, T. Sato, S. Fukao, and S. Kato (1990), Studies of velocity fluctuations in the lower atmosphere using the MU radar. Part I: Azimuthal anisotropy, *J. Atmos. Sci.*, *47*(1), 39–50.

Vincent, R. A., and I. M. Reid (1983), HF Doppler measurements of mesospheric momentum fluxes, *J. Atmos. Sci.*, *40*, 1321–1333.

Vincent, R. A., S. Kovalam, D. C. Fritts, and J. R. Isler (1998), Long-term MF radar observations of solar tides in the low-latitude mesosphere: Interannual variability and comparisons with the GSWM, *J. Geophys. Res.*, *103*(D8), 8667–8683.

Wang, D.-Y., and D. C. Fritts (1991), Evidence of gravity wave-tidal interaction observed near the summer mesopause at Poker Flat, Alaska, *J. Atmos. Sci.*, *48*, 572–583.

Wu, D. L. (2004), Mesoscale gravity wave variances from AMSU-A radiances, *Geophys. Res. Lett.*, *31*, L12114, doi:10.1029/2004GL019562.

Wu, D. L., and J. H. Jiang (2002), MLS observations of atmospheric gravity waves over Antarctica, *J. Geophys. Res.*, *107*(D24), 4773, doi:10.1029/2002JD002390.

Wu, D. L., and S. D. Eckermann (2008), Global gravity wave variances from Aura MLS: Characteristics and interpretation, *J. Atmos. Sci.*, *65*, 3695–3718, doi:10.1175/2008JAS2489.1.

Wu, D. L., P. Preusse, S. D. Eckermann, J. H. Jiang, M. de la Torre Juarez, L. Coy, and D. Y. Wang (2006), Remote sounding of atmospheric gravity waves with satellite limb and nadir techniques, *Adv. Space Res.*, *37*, 2269–2277.

Yuan, T., et al. (2006), Seasonal variation of diurnal perturbations in mesopause region temperature, zonal, and meridional winds above Fort Collins, Colorado (40.6°N, 105°W), *J. Geophys. Res.*, *111*, D06103, doi:10.1029/2004JD005486.

C. Brunini, Facultad de Ciencias Astronómicas y Geofísicas, UNLP/CONICET, San Juan, Argentina.

D. C. Fritts, H. Iimura, D. Janches, and R. G. Stockwell, NorthWest Research Associates, Colorado Research Associates division, Boulder, CO, USA. (dave@cora.nwra.com)

B. Fuller and B. Vandepeer, Genesis Software Pty Ltd., Adelaide, SA, Australia.

W. K. Hocking, Department of Physics, University of Western Ontario, London, ON, Canada.

J. Hormaechea, Estacion Astronomica Rio Grande (EARG), Universidad Nacional de La Plata (UNLP), Consejo Nacional de Investigaciones de Ciencoa y Tecnica (CONICET), San Juan, Argentina.

H. Levato, Instituto de Ciencias Astronomicas, de la Tierra y del Espacio (ICATE)/CONICET, San Juan, Argentina.

N. J. Mitchell, Center for Space, Atmosphere and Oceanic Science, Department of Electronic and Electrical Engineering, University of Bath, Bath, Avon, UK.